Change in Wind Renewable Energy Potential under Stratospheric Aerosol Injections

Susanne Baur, Benjamin M Sanderson, Roland Séférian, Laurent Terray

Change in Wind Renewable Energy Potential under Stratospheric Aerosol Injections

Susanne Baur[1], Benjamin M. Sanderson[2], Roland Séférian[3], Laurent Terray[1]

[1]CECI, Université de Toulouse, CERFACS, CNRS, Toulouse, France
[2]Centre for International Climate and Environmental Research (CICERO), Oslo, Norway
[3]CNRM, Université de Toulouse, Météo-France/CNRS, Toulouse, France

Corresponding author: Susanne Baur (susanne.baur@cerfacs.fr)

Key Points:

- Stratospheric Aerosol Injections have been proposed as a method to temporarily counteract the warming from greenhouse gases.
- Stratospheric Aerosol Injections do not compensate the atmospheric circulation changes from climate change but create new dynamics.
- Total global wind energy potential is negligibly reduced under Stratospheric Aerosol Injections but regional trends can be large.

Abstract

Wind renewable energy (WRE) is an essential component of the global sustainable energy portfolio. Recently, there has been increasing discussion on the potential supplementation of this conventional mitigation portfolio with Solar Radiation Modification (SRM). However, the impact of SRM on conventional mitigation measures has received limited attention to date. In this study, we explore one part of this impact, the potential effect of one type of SRM, Stratospheric Aerosol Injections (SAI), on WRE. Using hourly output from the Earth System Model CNRM-ESM2-1, we compare WRE potential under a medium emission scenario (SSP245) and a high emission scenario (SSP585) with an SRM scenario that has SSP585 baseline conditions and uses SAI to cool to approximately SSP245 global warming levels. Our results suggest that SAI may affect surface wind resources by modifying large-scale circulation patterns, such as a significant poleward jet-shift in the Southern Hemisphere. The modeled total global WRE potential is negligibly reduced under SAI compared to the SSP-scenarios. However, regional trends in wind potential are highly variable, with large increases and decreases frequently reaching up to 16 % across the globe with SAI. This study provides valuable insights into the potential downstream effects of SRM on climatic elements, such as wind patterns, and offers perspectives on its implications for our mitigation efforts.

1 Introduction

Wind renewable energy (WRE) is a key component of the transition to a low-carbon energy system (IPCC, 2018; Clarke et al., 2022; Riahi et al., 2022). Modeling assessments estimate that in Paris Agreement compatible scenarios, such as the C1 and C2 scenarios from the recent IPCC Assessment Report (Riahi et al., 2022), a significant portion of energy would come from wind with projected production ranging from 4,760 to 50,960 TWh/yr by 2050 depending on the scenario and model (Byers et al., 2022). However, present policies are taking us closer to a global mean surface temperature increase of 2.5-2.9°C than the Paris compatible 1.5°C (CAT, 2023), whilst current warming already leads to numerous climate change related damages (Ripple et al., 2023). Hence, a growing number of people are investigating a group of technologies, termed Solar Radiation Modification (SRM), as a potential addition to conventional mitigation, to rapidly manage climate change risks. SRM does not resolve the global warming problem as it does not eliminate greenhouse gases (GHGs), but is proposed to temporarily mask some of the impacts with

the logic of providing more time to sufficiently roll out mitigation measures and halt or reverse the rise of atmospheric GHG concentration (Horton, 2015; MacCracken, 2009; Royal Society, 2011; Schäfer et al., 2014). It works by modifying the balance of incoming and outgoing radiation in the Earth system, which, if done on a significant scale, can exert a global cooling effect to counteract warming due to greenhouse gases. SRM is perceived controversially by experts and laypeople alike (Müller-Hansen et al., 2023) due, in part, to the large social and ecological risks and unknowns involved in intentionally manipulating the complex Earth system.

Various proposals have been put forward to alter the radiative equilibrium, with the injection of aerosols into the stratosphere (SAI) receiving the most attention thus far. An SAI intervention aiming at global impact entails the continuous placement of aerosols at low latitudes in the lower stratosphere (Dai et al., 2018; Kravitz et al., 2019a; Tilmes et al., 2017; Tilmes et al., 2018b), where the Brewer-Dobson circulation slowly transports them towards the poles. The aerosols reflect the incoming short-wave radiation allowing less radiative energy to reach the surface. While this process leads to cooling at the surface, evidenced by large volcanic eruptions, not all radiation is reflected by the aerosols. Instead, some of the radiative energy is absorbed by the particles, leading to localized heating of the stratosphere, which can affect global circulation patterns (Baldwin & Dunkerton, 2001; DallaSanta et al., 2019; Stenchikov et al., 2002; Graft et al., 1993). For example, several studies on the impact of stratospheric aerosols from volcanic eruptions have found a poleward jet shift (Barnes et al., 2016; Polvani & Kushner, 2002; Simpson et al., 2009). This has been attributed to two general mechanisms, surface cooling and stratospheric warming (DallaSanta et al., 2019). The surface cooling from the stratospheric aerosols decreases the tropospheric meridional temperature gradient (Stenchikov et al., 2002; Graf, 1992), which reduces midlatitude baroclinity, driving a strengthening of the stratospheric vortex, which leads to a poleward shift of the jet (Baldwin & Dunkerton, 2001). The second and primary mechanism, however, is the observed warming of the stratosphere in the tropics due to the aerosol's absorption of the radiative energy. This enhances the stratospheric meridional temperature gradient leading to a strengthened stratospheric vortex that shifts the jet poleward (DallaSanta et al., 2019). Modeling studies on SAI impacts have also found large-scale circulation changes. Liu et al. (2023) studied the East Asian Winter Monsoon under SAI and found that aerosol injections reverse the weakening of the monsoon that occurs in SSP585. In Africa, however, SAI can lead to weaker monsoon winds (Da-Allada et al., 2020; Robock et al., 2008) and a slight southward shift of the

ITCZ (Cheng et al., 2019). It should be emphasized that the outcomes of these studies are likely strongly reliant on the selected injection design and the underlying model (Kravitz et al., 2016, 2019b; Lee et al., 2020; MacMartin & Kravitz, 2019).

Wind power generation relies significantly on local and regional wind patterns and even minor fluctuations in wind velocity can have a meaningful impact on the energy output (Veers et al., 2019). This is because the energy in the wind follows the cube of the wind speed. While to our knowledge no research has been conducted on WRE potential under SRM, several studies have looked at the impact of climate change on wind potential. They found significant alterations in wind velocity and its temporal distribution as a result of global warming (Solaun & Cerdá, 2019). One of the main mechanisms behind large-scale circulation changes from anthropogenic warming is the reduced equator-to-pole temperature gradient at the surface as a result from polar amplification, which is expected to alter tropical circulation (Ma et al., 2012), such as the Hadley cell, monsoon circulations and tropical cyclone frequency, as well as the behavior of midlatitude jet streams and storm tracks (Martinez & Iglesias, 2024; Pryor et al., 2020; Shaw et al., 2016). However, wind resources can be further impacted by ocean circulation and surface roughness changes from land cover modifications (Jung & Schindler, 2022; Vautard et al., 2010; Zeng et al., 2019). Additionally, local wind resources exhibit high variability on sub-hourly and multi-decadal scales (Jung et al., 2018). Due to the difficulty to accurately represent all drivers and the resulting temporal and spatial variations of wind patterns in Global Circulation Models, it is not entirely certain whether climate change will result in a decrease or increase in wind speeds at the global scale (Pryor et al., 2020). Most studies find highly diverse regional trends with large increases and decreases in wind speed and wind energy potential all over the globe (Gernaat et al., 2021; Jung & Schindler, 2022; Pryor et al., 2020; Solaun & Cerdá, 2019). As a result, on a global scale, changes in total wind energy density (Martinez & Iglesias, 2024) and wind energy potential (Gernaat et al., 2021) are small and may be slightly negative.

Given that WRE already plays an important role in the prevailing mitigation strategy, and that mitigation is an important aspect of ensuring the temporary use of SRM, it is important to understand whether SRM complements or conflicts with this existing method of energy generation and mitigation. Only through an understanding of the full spectrum of consequences from SAI can responsible decision-making be enabled. Here, we analyze the interplay between WRE and SAI

by calculating and comparing on- and offshore wind potential when SAI is used versus when mitigation has brought the climate to approximately the same GMST (SSP245). Additionally, we compare the SAI-modified climate with the fossil-fuel heavy emission baseline of the scenario without SAI (SSP585).

2 Model Experiments and Methods

2.1 Data and Simulations

This study is based on three experiments: a fossil-fuel intensive, high-emission scenario called SSP585 (O'Neill et al., 2016), a moderately ambitiously mitigated scenario, SSP245 (O'Neill et al., 2016), and a stratospheric aerosol injection (SAI) simulation that cools down from an SSP585 baseline to SSP245. The SAI experiment originates from the GeoMIP6 protocol (Kravitz et al., 2015) and is referred to therein as G6sulfur. We run these experiments from 2015 to 2100 in a 6-member ensemble with perturbed initial conditions on the CNRM-ESM-2.1 Earth system model (Séférian et al., 2019). Ensemble means are displayed except if defined otherwise. As a proxy for SAI we use prescribed aerosol optical depth derived from the GeoMIP G4SSA experiment (Tilmes et al., 2015) which scales up to 0.35 in the last decade of the simulation. The variables related to the directional winds u and v at 150m altitude are produced at hourly resolution on a 1°x1° grid. During the postprocessing we bilinearly regrid the climate model output to match the land use and land cover data (described in 2.2.3 Politico-economic dimension) which is on a 0.1°x0.1° grid. For the zonal winds we create two altitudinal categories: upper and surface. Upper refers to a pressure level of 200-400hPa, roughly corresponding to the upper troposphere, and surface, referring to a pressure level of 850-1050hPa, representing the air close to the Earth's surface.

2.2 Wind Potential Calculation

In the same manner as Baur et al. (2023), we use the term "potential" to refer to an enhanced version of the traditional definition of the "technical potential". The technical potential is the theoretical potential, here the surface wind resource, constrained by geographical and technical restrictions. In this study, we distinguish between three dimensions that are involved in the wind energy potential calculation: the technical dimension that establishes the technical restrictions to

the theoretical potential, the physical dimension, which is related to the energy extractable from surface wind speed, and the politico-economic one, which is related to the suitability of the grid cell i for wind turbine placement. We calculate the wind potential in a similar fashion to Gernaat et al. (2021) as:

$$TP_{i,loc} = Politicoeconomic_i \times Technical_{loc} \times Physical_{i,loc} \times gridcell_i \left[\frac{MWh}{yr}\right] \quad (1)$$

All parameters, their values, units and sources are given in Table S1. The subscript loc indicates whether it is an on- or offshore wind farm. The resulting electricity generation potential is expressed in various time slices, such as 10-year seasonal mean changes, weekly sums and yearly sums, calculated from the hourly wind speed input. Seasons refer to the four periods December, January, February (DJF), March, April, May (MAM), June, July, August (JJA) and September, October, November (SON). We calculate the Low Energy Week (LEW) metric as introduced by Baur et al. (2023).

2.2.1 Technical Dimension

This part of the calculation reduces the physical potential by accounting for the unavailability of the turbines due to maintenance, the wind farm array inefficiencies and the density of wind turbine placement. We use technical indicators from on- and offshore exemplary real-world wind turbines. To avoid projecting technological developments into the future we choose turbines which are either already or about to be in serial production but are at the forefront of current wind turbine development. We justify this choice with the argument that the average wind turbines of the future will be the most powerful wind turbines of today. Table 1 lists their characteristics:

Table 1. Exemplary on- and offshore wind turbine specifications. Data from Vestas (2023a), (2023b).

	Vestas V162-6.2 (onshore)	**Vestas V236-15** (offshore)
Rated power (P_r)	6.2 MW	15 MW
Cut-in windspeed (v_{ci})	3.0 m/s	3.0 m/s
Cut-out windspeed (v_{co})	25 m/s	30 m/s

Rotor diameter (d_{Rotor})	162 m	236 m
Serial production	2021	2024

The technical dimension consists of η_a, the annual availability of the turbine due to maintenance, η_{ar}, the wind farm array efficiency, and D_{loc}, the turbine density, and is a simple multiplication of these terms:

$$\mathrm{Technical_{loc}} = \eta_a \times \eta_{ar} \times \mathrm{D_{loc}} \left[\frac{\mathrm{turbines}}{\mathrm{km^2}}\right] \quad (2)$$

D is the average installed turbine density in the grid cell and is calculated as:

$$\mathrm{D_{loc}} = \frac{1}{(\mathrm{spacing} \times \mathrm{d_{Rotor,loc}})^2} \left[\frac{\mathrm{turbines}}{\mathrm{km^2}}\right] \quad (3)$$

We assume that turbine spacing is equal in prevailing and perpendicular wind direction. For the turbines set out in Table 1, this gives a $\mathrm{D_{onshore}}$ of 1.56 turbines/km2 and a $\mathrm{D_{offshore}}$ of 0.51 turbines/km2. Translated into the more commonly used metric power density, this implies 9.68 MW/km2 onshore and 7.65 MW/km2 offshore.

2.2.2 Physical Dimension

The physical dimension represents the power produced by a wind turbine p(v), which is described by the wind turbine power curve (Carrillo et al., 2013; Saint-Drenan et al., 2020; Fig S1) and calculated as:

$$p(v_i)_i = \begin{cases} 0 & v < v_{ci} \; or \; v > v_{co} \\ q(v_i) & v_{ci} \leq v < v_r \\ P_r & v_r \leq v \leq v_{co} \end{cases} \quad (4)$$

The power curve depends on the instantaneous wind speed v and the characteristics of the wind turbine (Table 1) and distinguishes between four different operation regimes (Fig S1): I, the area of wind speeds (v) that are smaller than the cut-in wind speed (v_{ci}), and therefore too low to produce any energy, II, the area of non-linear relationship between wind speed and power output ($q(v)$), III, the area of maximum power output, i.e. rated power (P_r), and IV, the area after the cut-

out threshold, where wind speed is too high ($v > v_{co}$) and turbines shut down to protect themselves from damage (Saint-Drenan et al., 2020; Wood & Wollenberg, 1996).

Power production in area II follows the parametric wind turbine power curve described in Saint-Drenan et al. (2020) and is calculated as:

$$q(v_i) = 0.5 \times \rho \times \varepsilon_{loc} \times v^3 \times pc \left[\frac{MWh}{turbine}\right] \quad (5)$$

With ρ being the air density, which is kept constant, ε the area swept by the rotor blades calculated from the rotor blade diameters (Table 1), v instantaneous wind speed and pc the power coefficient, a measure for aerodynamic-mechanical-electrical performance of the turbines (Veers et al., 2019). For simplicity, in our study, the power coefficient is held constant, however, as demonstrated in Saint-Drenan et al. (2020), it is ultimately dependent on and varies with the wind's velocity. The power coefficient parameterization leads to a slight overestimation in power output from higher wind speeds and underestimation of output from lower wind speeds in the $q(v_i)$-part of our calculation.

Due to the high variability of wind, a temporal resolution of 1 hour and a spatial resolution of 1°x1° may not adequately represent all prevailing wind speeds in the area during the specified time period. To account for the requirement of instantaneous wind velocity in the wind power curve calculation and the low spatial resolution of the input data, we represent wind speed through a probability density function. Weibull distributions have frequently been used to represent the spread in wind speed over a time period at a given location (e.g. Aukitino et al., 2017; Mohammadi et al., 2016; Shi et al., 2021; Shu et al., 2015) and as a means of downscaling to represent the spread of wind over a larger area (Alizadeh et al., 2020; Chang et al., 2015; Tye et al., 2014; Zhou & Smith, 2013). The temporal resolution of the underlying wind data can range from 10 min (Eskin et al., 2008), to hourly (Chang et al., 2015; Li et al., 2020; Mohammadi et al., 2016; Burton et al., 2001), 6-hourly (Elsner, 2019), to daily (Shu & Jesson, 2021) and longer. Cradden et al. (2014) and Pryor et al. (2020) have highlighted the importance of a high temporal resolution of at least 1 hour for WRE analyses. Although hourly and daily average wind speeds have been shown to lead to similar power output results from a turbine over a long time period, hourly input data is much better at representing the peaks and lows during the day and can give a more precise result for shorter time periods (Shin et al., 2018; Veronesi & Grassi, 2015; Justus et al., 1978). In this study,

the Weibull distribution is used to represent sub-grid spatial and temporal variation in wind. We use a constant shape-parameter for all regions across the globe. This is a frequently applied simplification (Dvorak et al., 2010; Elsner, 2019; Eurek et al., 2017; Shu et al., 2015; Sohoni et al., 2016; Valencia Ochoa et al., 2019; Arendt et al., 2013) related to the width of the distribution and therefore the gustiness of the wind regimes (Eurek et al., 2017) that is most commonly used in larger scale analyses. Studies have demonstrated variation of the shape parameter across regions (Zhou & Smith, 2013), especially for oceanic winds (Shi et al., 2021; Perrin et al., 2006). However, apart from coastal areas, oceanic regions are excluded from this analysis and using the Rayleigh-form of the Weibull distribution, which sets the shape parameter β to 2 and implies moderately gusty winds across all areas (Eurek et al., 2017), drastically reduces the computational effort. The scale parameter, α, is calculated according to Lysen (1983) as follows:

$$\alpha = ws_i \times (0.568 + 0.433 \times 0.5)^{\frac{1}{\beta}} \quad (6)$$

with ws_i being the hourly wind speed from our model output calculated as the square root of the sum of the squares of the east- and northward wind components u and v. We calculate $p(v)$ for all 1000 samples in the Weibull distribution for each 1 m/s wind speed bin from 0-50 m/s.

The 2-parameter Weibull distribution representing the range of wind speeds prevalent in the 1-hour mean 1° grid cell model output is calculated as:

$$\mathrm{f(T)} = \frac{\beta}{\alpha} \times \left(\frac{\mathrm{T}}{\alpha}\right)^{\beta-1} \times \mathrm{e}^{-\left(\frac{\mathrm{T}}{\alpha}\right)^{\beta}} \quad (7)$$

For computational feasibility we fit a curve between the 1-hour mean wind speed and the power output, i.e., $p(v)$, that takes into account the Weibull spread of wind speed and the turbine power curve:

$$Physical_{i,loc} = p(ws_i)_{loc} = a_{loc} \times \left(1 - e^{\frac{-ws_i{}^2}{b_{loc}}}\right) \times \left(1 - e^{\frac{-ws_i{}^2}{c_{loc}}}\right) \times e^{\frac{-ws_i}{d_{loc}}} \left[\frac{MWh}{turbine}\right] \quad (8)$$

Please consult Table S1 in the SI for the values of the parameters a_{loc}, b_{loc}, c_{loc} and d_{loc}. To assess how much energy is lost due to a change in the distribution of hourly wind speeds we additionally calculate the wind potential without the cut-out wind speed limit (no-cut-out). Instead, power output at $v > v_{co}$ is kept at P_r. By subtracting the yearly cumulative "standard"-turbine-

power-curve power output with the output from these no-cut-out calculations, we can estimate the amount of TWh that is gained or lost in a year due to a change in fast winds. Figure S2 shows the fitted power curve of an onshore and offshore grid cell in the normal setting and in the no-cut-out-setting.

2.2.3 Politico-Economic Dimension

The incorporation of a politico-economic dimension is a long-standing approach for wind potential calculations (e.g. Eliott & Schwartz, 1993; Archer & Jacobson, 2005; Bosch et al., 2017; Hoogwijk, 2004; Zhou et al., 2012) and is related to the suitability of each grid cell to harbor wind turbines. Various parameters have been taken into account in the past. Here, we consider surface properties and land use competition for our onshore wind farms as done in Baur et al. (2023). Figure 1 displays the convolutions of the single area restrictions for on- and offshore wind farms which are used in the wind potential calculation ($Politicoeconomic_i$). The single area restrictions and their weights are displayed in Figure S3 and S4. We exclude all areas marked as protected with any status as characterized by the United Nations Environment Programme (IUCN, 2023) as possible wind power installation sites and weigh areas according to the prevalent land-use and distance to highly populated centers as an indicator for the future existence of transmission lines and demand. Highly populated areas are excluded since wind turbines are rarely situated in close proximity to, or on top of, buildings. For offshore we add additional constraints, such as the bathymetry over 1000m, exclusion of grid cells outside the Exclusive Economic Zone (EEZ) (Flanders Marine Institute, 2019) and consideration of only those grid cells that are at least 95% sea-ice free in every season of the year.

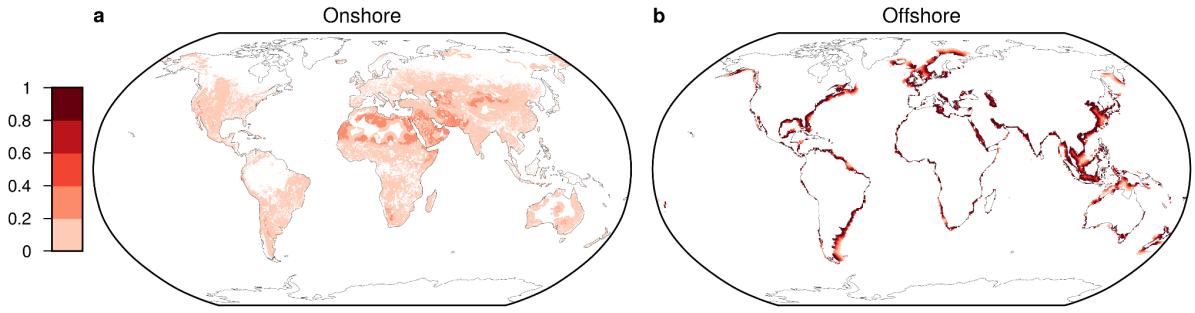

Figure 1. Convolution of area restrictions for a) onshore and b) offshore.

Land-use cover and population density data were obtained from the IMAGE3.0-LPJ model (Doelman et al., 2018; Stehfest et al., 2014) with a spatial resolution of 0.1°x0.1°. The model

differentiates between 20 different land use and land cover categories. We weigh each type according to the fraction of a grid cell that could be covered by wind farms, in line with Baur et al. (2023), but with different fractions assigned (see Table S2 for land use categories and assigned suitability fractions). The rationale behind the suitability fraction is that only part of a grid cell is available for wind farms as they could potentially conflict with other land uses such as cities, agricultural production or ecosystem services from forests. A suitability fraction of 15% denotes that 15% of the grid cell is able to accommodate a wind farm. The spacing between the turbines of several hundred meters enables a certain level of coexistence between wind farms and predominant land uses. This explains the assignment of higher fractions for, for example, agricultural areas in this study than in Baur et al. (2023), which looked at solar farms.

We use the same approach as Baur et al. (2023) to weigh the proximity to highly populated areas. The population data from the IMAGE3.0 LPJ model consists of 5-year intervals and is aggregated to 10-year means for our analysis (Doelman et al., 2018; Stehfest et al., 2014). Using a sigmoidal function, we impose that the weight diminishes proportionally as the distance to densely populated cells grows, ultimately tapering to zero at approximately 500 km. Unlike Baur et al. (2023), we exclude highly populated areas, which we define as cells where population density is larger than 1000 inhabitants/km2.

We present results that are calculated using equal weights across all scenarios and time intervals. Therefore, the data underlying population, sea ice and land use are related to the 2090-2099 time frame of SSP245 but are used as a basis for all three scenarios.

3 Results

3.1 Large-scale Circulation Response to SAI

Our simulations indicate substantial alterations in 10-year mean zonal wind from the present (2015-2024) to the end of the century (2090-2099) (Fig S5). While the patterns of change show some similarities for SAI, SSP585 and SSP245, the magnitude of the circulation differences from present to future varies considerably and is especially pronounced for SAI and SSP585 (Fig S5). When comparing the future conditions of the scenarios with each other, substantial differences become apparent (Fig 2). Regardless of altitude or scenario-comparison, the largest differences are registered in the Southern Hemisphere (SH): Here, the westerlies' shift towards the pole is more

pronounced under SAI compared to the SSP-scenarios and, comparing the SSP-scenarios, there is a more intense strengthening of the westerlies and poleward shift of the SH jet for SSP585 compared to SSP245 at the end of the century. The signal is strongest in the upper troposphere for all scenario-comparisons with differences in zonal wind speed of up to 4 m/s (Figure 2 a-c). While the sign of difference between SAI and the SSPs stays consistent across most seasons, the intensity varies (Fig S6, S7).

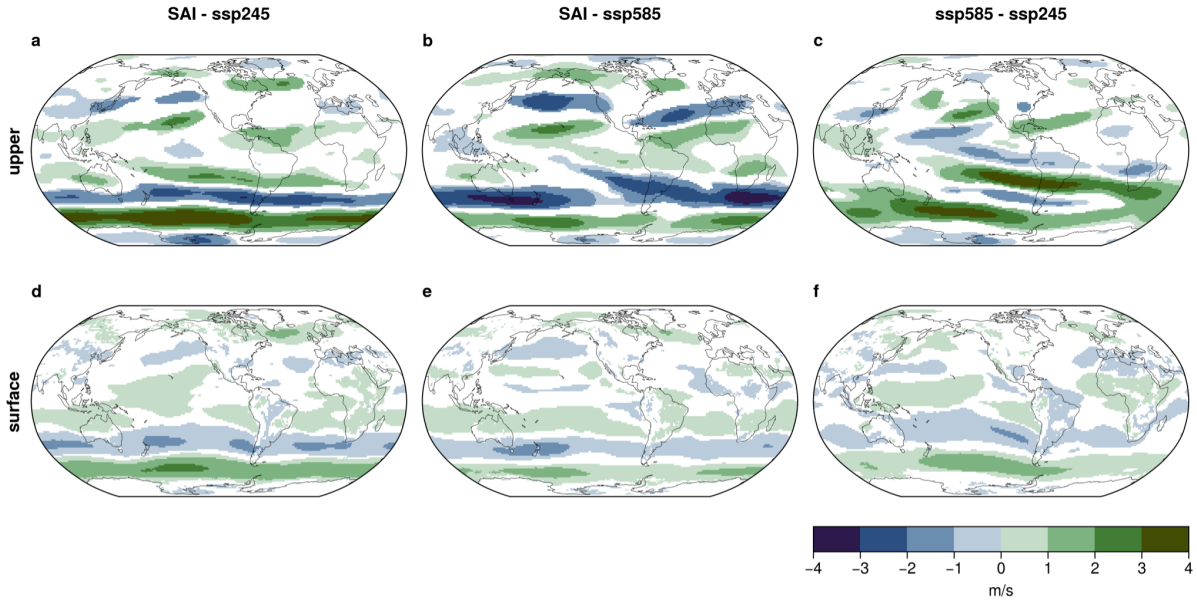

Figure 2. Difference in 2090-99 mean zonal winds between a,d) SAI and SSP245, b,e) SAI and SSP585 and c,f) SSP245 and SSP585 at a-c) the upper troposphere and d-f) the surface.

In the NH, the changes are less latitudinally and, over the Atlantic Ocean, altitudinally consistent. While both upper tropospheric and surface winds show a pronounced equatorward shift of the midlatitude westerlies over the Pacific under SAI compared to the SSPs, the upper troposphere over the Atlantic entails a strengthened equatorward shift of the subtropical jet that does not propagate as much to the surface as for the SH (Fig 2, 3, S5). The decrease in midlatitude wind speed under SAI moves towards the equator as it propagates to the surface when comparing to SSP245, while shifting slightly poleward when comparing to SSP585 (Fig 3 a,b). The largest circulation changes occur in the upper troposphere and stratosphere (Fig 2, 3).

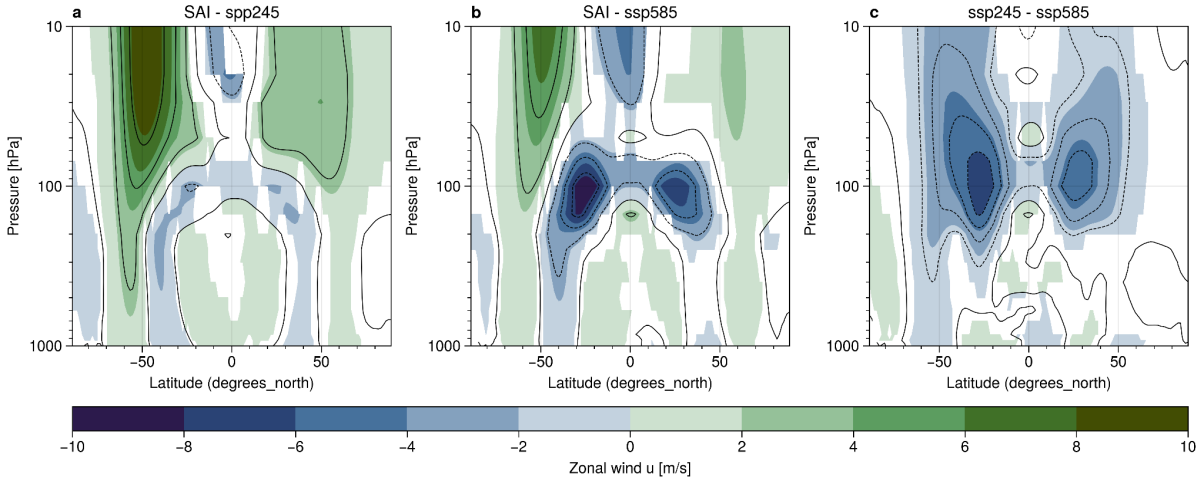

Figure 3. Difference in 2090-99 average zonal mean winds between a) SAI and SSP45, b) SAI and SSP585 and c) SSP245 and SSP585.

Variation in large-scale circulation has been attributed to temperature changes in the stratosphere and resulting increases or decreases in the temperature gradients at the surface and/or the upper troposphere (Baldwin & Dunkerton, 2001; Charlesworth et al., 2023; DallaSanta et al., 2019; Simpson et al., 2019; Stenchikov et al., 2002; Graf, 1992). In our simulations we see a large temperature shift of up to 14K under SAI compared to the SSP-scenarios in the tropical stratosphere (Figure S8). The largest increase is at around 80hPa. As expected, temperatures at the surface are lower under SAI than SSP585, especially in the tropics, which is a common phenomenon observed in SRM simulations. Due to the augmented CO2 concentration, which increases the rate that the stratosphere radiates heat to space, the stratosphere is colder under SSP585 than SSP245 (Figure S8c).

Long-term average wind speed is substantially lower in the NH under SAI compared to the present (Fig 4a) and compared to the SSPs (Fig 4d,e). A trend fairly consistent throughout the scenarios but most noticeable in SSP585 is the increase in wind speed in tropical land regions compared to the present, especially in Brazil and on the African continent. Most other land regions experience reductions in wind speed (Fig 4a-c).

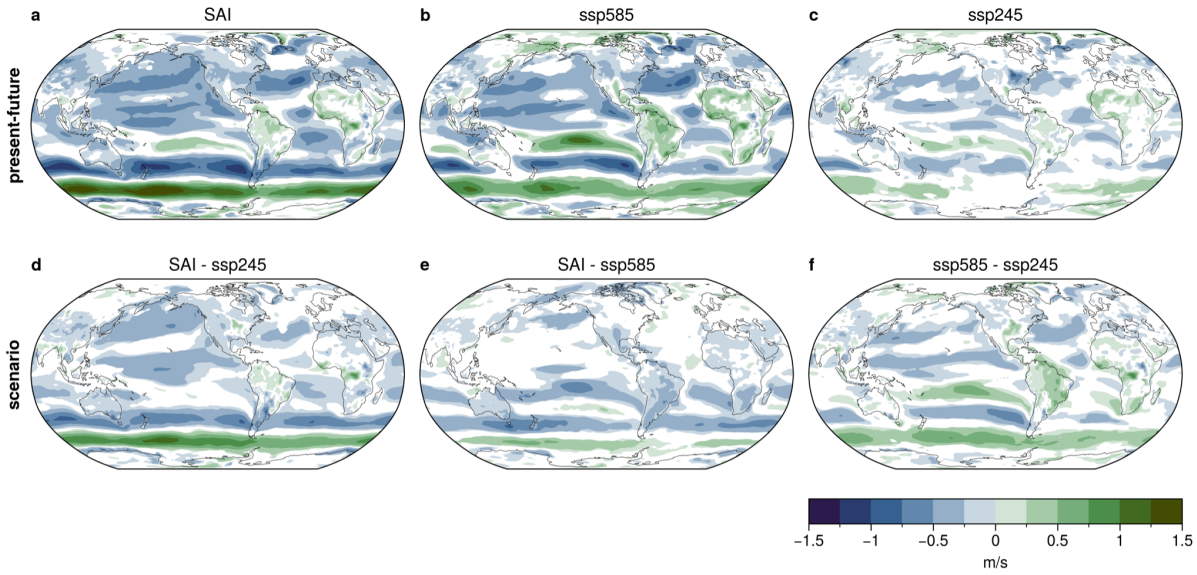

Figure 4. 150m wind speed comparing present (2015-2024) and future (2090-2099) states under a) SAI, b) SSP585 and c) SSP245 and comparing future states of scenarios d) SAI and SSP245, e) SAI and SSP585 and f) SSP585 and SSP245.

3.2 SAI effect on onshore and offshore wind potential

Results in this part are presented with respect to three different areas of interest: long-term relative seasonal changes, changes in extended low-energy periods (LEW) and the effect of changes in high hourly wind speed on annual energy production.

Figure 5 displays the relative difference in 2090-99 seasonal wind potential between the SSP-scenarios and SAI (see Figure S9 for 10-year mean present to future comparisons for each scenario). The sign of change is relatively consistent, although varying in strength, through the different seasons for SSP245 -> SAI, except for the South East Asian and Northern European region, where DJF and MAM show a large increase in wind potential, while JJA and SON show a decrease (Fig 5a,d,g,j). The same seasonal pattern is visible for SSP585 -> SAI in South East Asia, but not in Europe. In general, the seasons appear to agree less on the sign of the relative change between SSP585 and SAI than for SSP245 and SAI. For example, apart from Europe and South East Asia, also Central Africa and Central Asia show different trends depending on the season when comparing SSP585 with SAI (Fig 5b,e,h,k). While there is not one single region that stands out with especially large differences compared to others, the most pronounced differences in SSP585 to SAI of around 16% are the large decrease in JJA in the southern Sahara (Fig 5h), the decrease in northern China in DJF (Fig 5b), the decrease in South America through all seasons but especially in Brazil in SON (Fig 5k) and Argentina, Bolivia and Paraguay in DJF (Fig 5b) and the

346 increase in South East Asia and the Chad and Sudan area in the south-east of the Sahara desert in
347 DJF (Fig 5b). For SSP245 to SAI, Central Asia sees a significant decrease through all seasons but
348 especially in DJF (Fig 5a). DJF furthermore indicates a large increase for southern South East
349 Asia, northern offshore Australia and Central and South-East Brazil (Fig 5a). In MAM, East Brazil
350 shows a big decreasing signal (Fig 5d). The SON months see a large increase in potential under
351 SAI for Myanmar and Central/North India (Fig 5j). While the regional differences are diverse and
352 large, globally, relative differences are small. SAI potential is only 2.2 % lower onshore and 1.3
353 % lower offshore than for SSP245 and 3.0 % lower onshore and 0.9 % lower offshore than for
354 SSP585. Between the SSP-scenarios the total global relative difference ends up being 0 % since
355 onshore potential is increased under SSP585 compared to SSP245 by 0.6 % but onshore potential
356 decreased by 0.6 %.
357

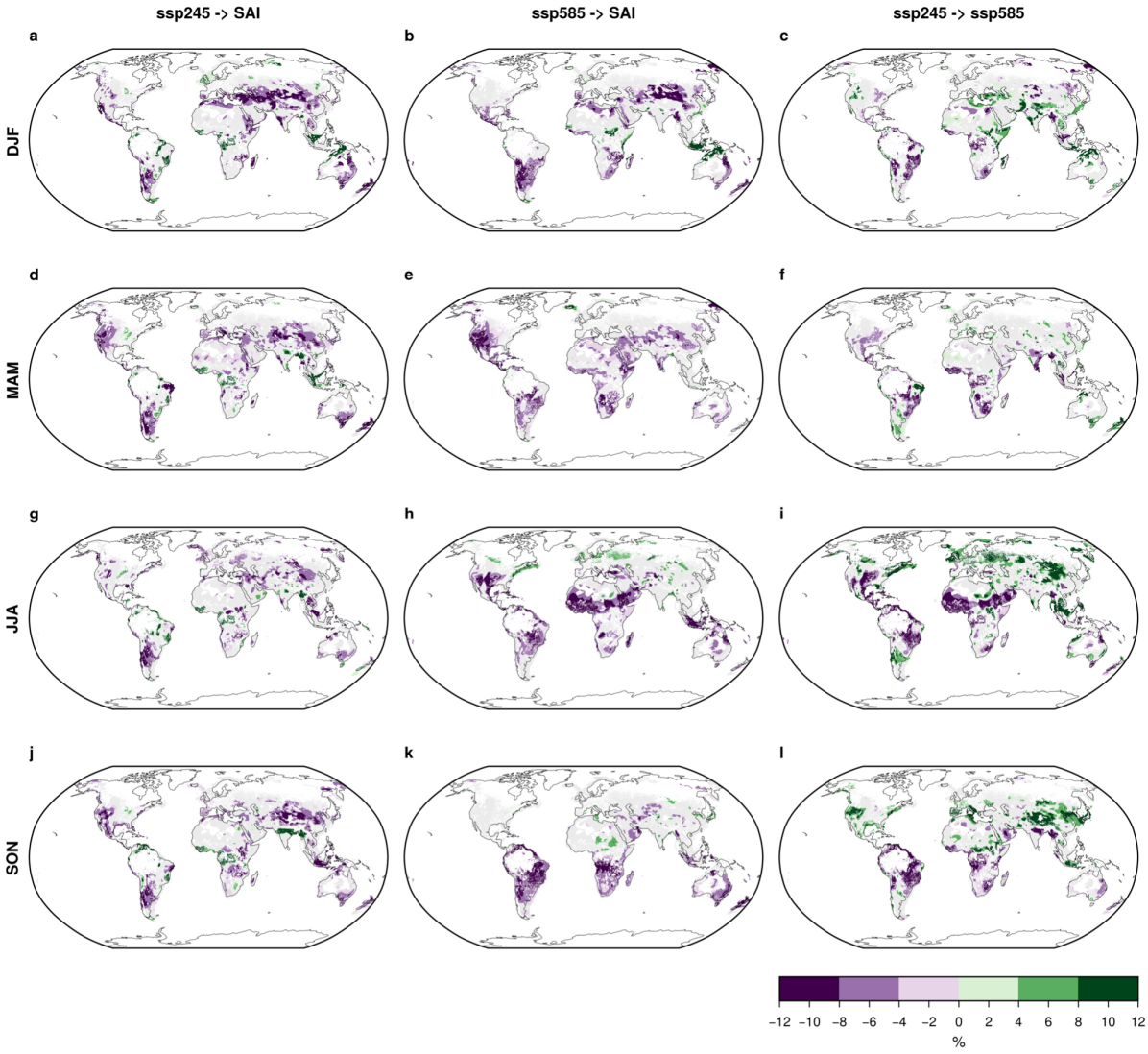

Figure 5. Relative differences in seasonal 2090-2099 wind potential for a,d,g,j) SSP245 to SAI, b,e,h,k) for SSP585 to SAI and c,f,i,l for SSP245 to SSP585 in the seasons a-c) December, January, February (DJF), d-f) March, April, Mai (MAM), g-i) June, July, August (JJA) and j-l) September, October, November (SON). Colored areas are statistically significant $p<0.05$, gray areas are considered suitable for wind production but show no significant change. x -> y denotes (y – x)/x.

The LEW metric assesses which regions experience prolonged periods of particularly low energy production. Figure 6 displays the number of weeks per year in SAI, SSP585 and SSP245 that have a wind energy output below the current (2015-2024) 20th seasonal percentile. Areas with up to 10 weeks per year imply that they stay unchanged in terms of low energy weeks or have less than in the present. Apart from some small areas in central South America and central China, globally, most areas see a slight increase in LEWs regardless of the scenario. West Africa, parts of the

Arabian Peninsula and south-east Brazil see no change or a decrease in LEWs in all scenarios. However, when comparing the scenarios with each other and refining the color-coding, substantial differences become apparent (Fig 6d-f). SAI leads to an increase of more than 6 additional LEWs per year compared to SSP245 or SSP585 in large parts of southern South America, south-east Australia, Central Asia and the Middle East. At the same time, many regions see less LEWs with SAI than with the SSP-scenarios. For example, compared to SSP245, the Great Plains in the US, several areas in Brazil, South Africa, West Africa, parts of the Arabian Peninsula, Myanmar and India and north-east Australia seem to benefit from SAI in terms of LEW count. Compared to SSP585, SAI appears to be especially advantageous in the north-east of North-America, northern Europe, the Arafura and Timor Sea between Australia and Indonesia/Timor and some regions in central China.

With some exceptions, such as north-east Australia, South Africa, northern Russia, offshore north-east North America and offshore Indonesia, the sign and magnitude of change stays consistent with the LEWs and the 10-year averages for SAI compared to SSP245 (Fig 6d, S10a). Similar for SAI versus SSP585, where exceptions are in the offshore area of north-east North-America, Mexico and southern US, offshore Borneo, Myanmar and South America, especially Argentina (Fig 6e, S10b).

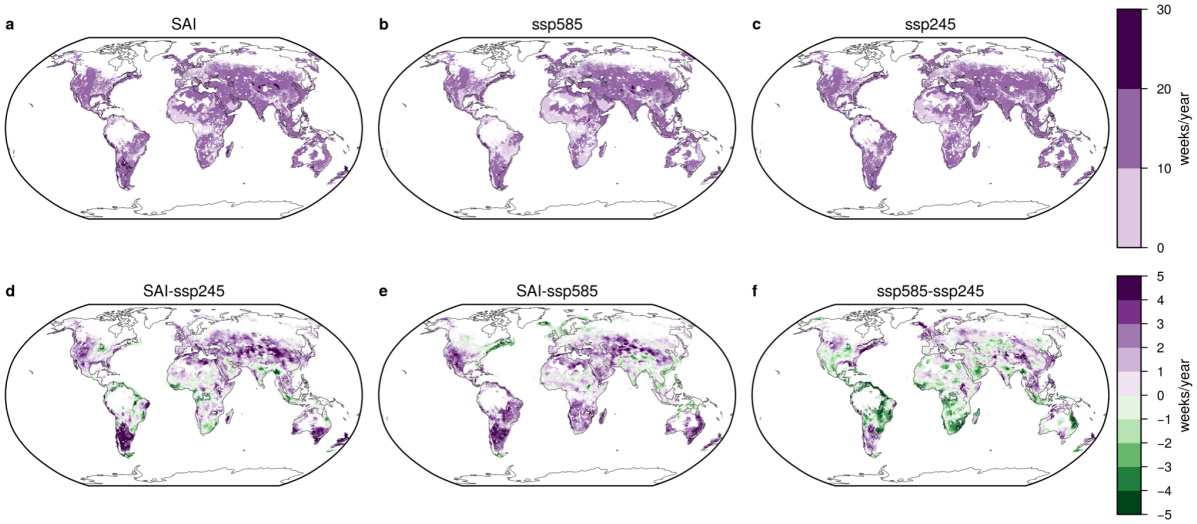

Figure 6. Low Energy Week (LEW) metric for a) SAI, b) SSP585 and c) SSP245. The LEW is calculated between the present (2015-2019) and the future (2095-2099). See Baur et al. (2023) for the LEW equation. d-f) are the differences between a-c).

To evaluate how much of the changes in wind potential are caused by changes in fast wind speed, we measure the annual power loss resulting from winds exceeding the cut-out threshold. Figure 7 shows which areas are mostly affected by energy losses due to fast winds in GWh per year per grid cell. Unsurprisingly, offshore areas are mostly affected by losses due to fast winds since wind is generally significantly slower over land areas (Fig 7a-c) and we applied lower suitability restrictions on offshore than onshore grid cells. Nevertheless, there are several onshore areas that see substantial reductions, such as the Great Plains in the US, the Southern parts of the Sahara, Central Asia and Russia. The differences between the scenarios are displayed in Figure 7d-f. Offshore northern Europe, the tip of Argentina and eastern Canada are the only regions that have substantially higher losses due to fast winds under SAI than the SSP-scenarios. SAI makes winds offshore of China, eastern USA, New Zealand and south-east South America and, onshore, the Sahara more accessible to energy generation. The total global energy loss due to fast winds is lowest for SAI with 8.5 PWh/yr (2.6 %) and identical for SSP245 and SSP585 with 8.9 PWh/yr (2.7 %).

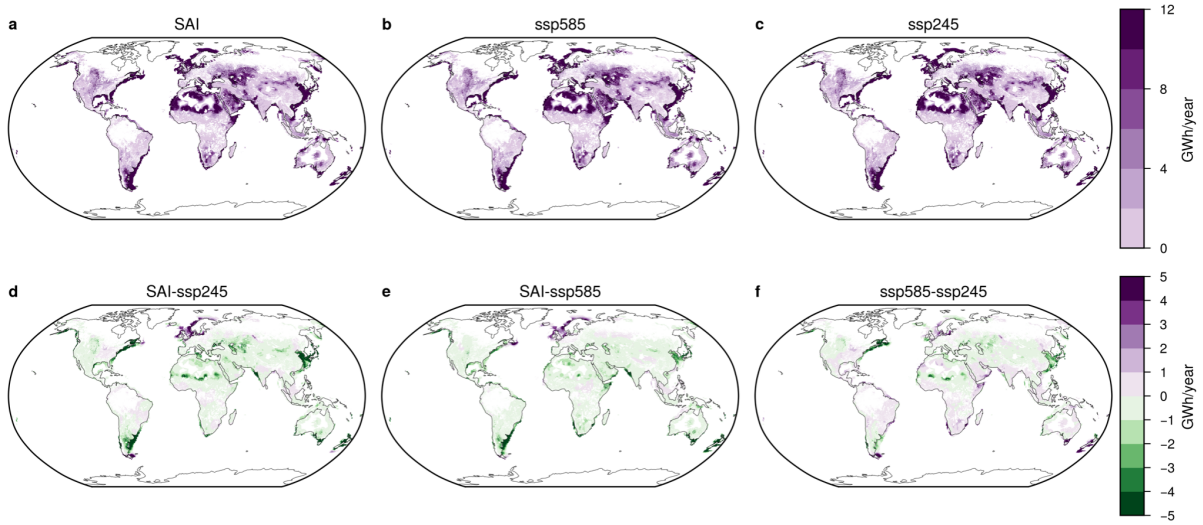

Figure 7. Difference between normal power curve setting and "no-cut-out" power curve setting for a) SAI, b) SSP245 and c) SSP585. Differences in energy lost due to fast winds between a) SAI and SSP245, b) SAI and SSP585 and c) SSP585 and SSP245.

4 Discussion

In this study, we examined the interplay between Stratospheric Aerosol Injections (SAI) and renewable wind energy potential. We found large changes in wind potential under SAI compared to a medium emission (SSP245) or high emission (SSP585) climate state depending on

the season and region (Fig 5, 6). The change in potential under SAI is especially regionally highly diverse with magnitudes frequently reaching 16 %. These large regional differences average out to a total global potential that is slightly smaller than for SSP245 or SSP585.

Wind energy potential is highly dependent on wind resources and long-term changes therein are mainly due to large-scale atmospheric circulation (Jung & Schindler, 2022). Previous analyses on stratospheric aerosols and atmospheric circulation have found impacts on global and regional circulation patterns, in particular a poleward shift of the jet (Barnes et al., 2016; McCusker et al., 2014; Polvani & Kushner, 2002; Simpson et al., 2009, 2019). In our analysis, we also found significant differences in zonal wind between SAI and the SSP-scenarios, as well as under the SSP-scenarios themselves (Fig 2, 3). The largest disparities exist within the Southern Hemisphere (SH) westerlies, which show a poleward shift under SAI compared to the SSP-scenarios, leading to both an increase and a decrease in the zonal mean wind of up to 4 m/s (Figure 2, 3). Our results are in agreement with those of Simpson et al. (2019), who studied alterations in large-scale circulation patterns using an SAI-setup known as GLENS. GLENS uses SAI to stay at 2020 conditions under an SSP585 baseline (Tilmes et al., 2018a). Simpson et al. (2019) conducted separate isolated forcing experiments to analyze how shifts in zonal wind patterns are driven by the stratospheric temperature change from SAI in GLENS. The authors note westerly stratospheric anomalies in the extra-tropics of similar magnitude and pattern as those identified in our study, and attribute the dominant role driving this change in the SH to the heating of the tropical lower stratosphere, an effect likewise observed in our experiments (Figure S8). Studies on stratospheric aerosols from volcanic eruptions and circulation anomalies have made the same observation (Barnes et al., 2016; DallaSanta et al., 2019; Karpechko et al., 2010; McGraw et al., 2016; Graft et al., 1993; Kirchner et al., 1999) and attribution to stratospheric heating (Barnes et al., 2016; DallaSanta et al., 2019; Polvani & Kushner, 2002; Simpson et al., 2009). However, not all volcanic modeling results lead to the same conclusion: In the Northern Hemisphere (NH), Ramachandran et al. (2000) and Marshall et al. (2009) find an equatorward shift in response to the volcanic forcing instead and in the SH Robock et al. (2007) and Roscoe & Haigh (2007) found no or a slight equatorward shift. Simpson et al. (2019) and McCusker et al. (2015) observe, and our study confirms, that the SH shows a much stronger signal, and that not all the changes in the NH are attributable to the stratospheric heating, such as, for example, in the North Pacific or the Atlantic during JJA (Simpson et al., 2019).

Tang et al. (2023) noted a total global reduction in onshore wind speed as a side effect of SAI using the same underlying scenarios as this study, but a different model and a lower temporal resolution. They see similar spatial patterns and magnitudes of change in surface wind speed as we do (Fig 5l-k in Tang et al., 2023), especially over land (Fig 4e), and results from regional analyses also broadly overlap with our findings (Da-Allada et al., 2020; Mousavi et al., 2023). However, Xie et al. (2022) used a 6-model ensemble to identify the impacts of SAI on the Atlantic Meridional Overturning Circulation and report changes in global wind speed patterns as a result of SAI that are different from ours. The divergence in results may be partially explained by the difference in scenario comparisons but it nevertheless suggests that the impacts of SAI on wind are not well understood to date. The scenario-comparisons in Figure 4 and 5 suggest that SAI does not compensate for changes from global warming but modifies wind resources in a novel way.

While no studies exist to date that evaluate wind energy potential changes under SRM, studies looking at changes in WRE potential due to climate change have found regionally highly diverse trends (e.g. Gernaat et al., 2021; Solaun & Cerdá, 2019; Tobin et al., 2015). We generally see similar developments for the SSP245 and SSP585 comparison as other studies that look at wind potential under climate change. Remarkable similarities exist on the South American (De Jong et al., 2019; Gernaat et al., 2021; Pereira De Lucena et al., 2010; Pereira et al., 2013) and African continent (Gernaat et al., 2021; Sawadogo et al., 2021) and Europe (Carvalho et al., 2017; Davy et al., 2018; Gernaat et al., 2021; Tobin et al., 2015, 2018).

Gernaat et al. (2021) note a relative global reduction in offshore wind potential of 2.1 % from historical (1970-2000) values to the end of the century under an RCP6.0 pathway and a reduction in onshore potential by 4.1 %. This is much higher than what we see for SSP245 versus SSP585, which has a global mean reduction in onshore wind potential of 0.6 % and an increase in offshore potential of 0.6 %. Our analyses are not directly comparable due to differences in underlying data and methodology and because our pathways result in a greater level of warming at the point of comparison. However, the absolute temperature difference between SSP245 and SSP585 and Gernaat et al.'s historical and end-of-century value is of similar range. Despite the much smaller relative global change in potential with climate change compared to Gernaat et al.'s study, we calculate a total global potential that is broadly comparable with the results from Gernaat et al. and other studies that provide wind technical potential in energy units (Table 2; Archer & Jacobson, 2005; Bosch et al., 2017; Chu & Hawkes, 2020; Eurek et al., 2017; Gernaat et al., 2021; Hoogwijk,

2004; de Vries et al., 2007; Lu et al., 2009; Krewitt et al., 2009). Discrepancies are possible due to differences in the underlying models, unalike methodological approaches in calculating the potential, such as dissimilar assumptions regarding land suitability and the characteristics of the wind turbines, as well as the temporal resolution of the wind data. Contrary to those studies, our offshore potential is much greater than onshore, and energy losses offshore are also much higher than onshore (Figure 7). This is due to the stronger suitability constraints we apply on land grid cells and, as demonstrated by Martinez & Iglesias (2024) and Tian et al. (2019), the generally higher energy density offshore.

Table 2. Comparison of total global on- and offshore wind potential with previous studies. Our results: SSP245 in 2090-2099 based on yearly sums of hourly output. NA means not available.

	Onshore [PWh/yr]	**Offshore** [PWh/yr]	**Area**	**Year**
Our results	217	399	global	2090-2099
Hoogwijk, 2004	96	NA	global	2000
de Vries et al., 2007	34	NA	global	2000 / 2050
Krewitt et al., 2009	105	16	global	2050
Eurek et al., 2017	560	315	global	NA
Chu & Hawkes, 2020	211	216	global	NA
Bosch et al., 2017	587	330	global	NA
Lu et al., 2009	690	157	global	2000
Archer & Jacobson, 2005	630	NA	global	2000
Gernaat et al., 2021	149	114	global	2070-2100

The LEW metric assesses whether an area encounters notably low weekly energy production variations, tackling the intermittency apprehension of RE. Extended durations of considerably low production, as measured by the LEW metric, may be more significant than a minor decline from high production days to medium production days, as indicated by long-term average data. Several areas all over the globe see up to 6 additional or 6 fewer LEWs per year on average under SAI than the SSP-scenarios (Figure 6). The regional sign and magnitude of change mostly overlaps with that from the 10-year average changes (Figure S10). Baur et al. (2023) computed the LEW metric for Photovoltaic potential under SAI and found much larger increases in the order of up to

12 additional LEWs per year under SAI compared to SSP245 and less agreement on the sign and magnitude of change between long-term average and LEW difference. While their change in LEWs is much higher than what we see for wind, their relative decrease in long-term averages is much lower. This means that in those weeks where energy production is low for wind RE, it is particularly low, pulling the long-term average to higher numbers. Whereas for Photovoltaic potential, the LEWs are frequent but not as unproductive. Since long periods of calm winds or cloudy conditions can be problematic for energy systems that rely on wind or solar RE, it is relevant to look at whether regions with high general wind potential and high LEW increase correlate with regions of high solar potential and high solar LEW increase or trends in other types of intermittent renewable energies.

Wind turbine energy output does not scale linearly with wind speed. Rather, they have a delicate range of wind speeds in which they can produce electricity, described by the wind turbine power curve. Hence, lower (higher) wind speeds do not necessarily imply lower (higher) wind potential. Nevertheless, in our analysis, with the same time periods considered, the maps of differences in wind potential (Figure S9) correlate well (correlation coefficient 0.68 for SAI; 0.70 for the SSP-scenarios) with the maps of differences in wind speed (Figure 4). However, while total global potential is smaller under SAI than in the SSP-scenarios, SAI reduces the amount of energy that is lost due to fast winds that are not harvested by wind turbines (Fig 7). The observed decrease in WRE potential under SAI can therefore not be attributed to alterations in fast wind patterns and the current quest for wind turbines with ever-higher cut-out thresholds might take up a lower priority in an SAI-modified world. The total amount of energy lost due to fast winds for all three scenarios in our results is likely to be smaller than real-world applications would suggest, partly due to the Weibull distribution we apply to power output to represent variations in wind speed over time and space. This distribution results in power outputs for 1-hour average wind speeds that are above the cut-out wind speed (Fig S2), because even if the average wind speed is above the cut-out threshold, some samples of the Weibull distribution of that average wind speed may be below the cut-out and therefore produce electricity. In reality, however, the wind turbines are not instantly turned on and off for wind gusts above or below the cut-out threshold. This means that we could be overestimating the energy gained and underestimating the energy lost from fast winds. However, the wind turbine power curve represents the power output of a single turbine, and our positively-skewed normal distribution of power output may a better representation of the output

from an entire grid cell, as other studies have shown (Bosch et al., 2017; Pryor & Barthelmie, 2010).

Wind varies greatly in space and time (Cradden et al., 2014; Lee et al., 2018; Yan et al., 2020) and our hourly input data, which represents entire 1° grid cells, is not able to fully reflect that. We regridded our wind data using a bilinear method to match the spatial resolution of the land use data rather than conducting a costly statistical downscaling. As an approximation of the different wind speeds in space and time we applied a Weibull distribution. A constant Weibull shape parameter was used across the globe to ensure computational practicality. However, this approach may lead to under- or overestimation of wind power output in certain regions (Zhou & Smith, 2013). Selecting a constant shape parameter in the Weibull distribution is a simplification because it ultimately relies on the regional wind system and terrain. Nevertheless, any errors that may be produced from this simplification will affect all three scenarios equally and will be largely negated when comparing the scenarios. Our study focuses on the impact of SAI on wind renewable energy potential, specifically differences in predicted future states rather than precise and accurate regional representations of wind potential.

The study's findings are specific to a single SAI experimental set-up (continuous injection of sulfate aerosols) and model that may have a larger SAI signal than is currently considered in a hypothetical deployment scenario but allows us a larger signal-to-noise ratio. Since no other modeling groups have performed SAI experiments with hourly wind output, the study's robustness is constrained by these limitations. However, several studies looking at surface wind speed changes under SAI have found similar patterns to us (Da-Allada et al., 2020; Mousavi et al., 2023; Tang et al., 2023). To increase the robustness of the results, more model intercomparison studies such as Xie et al.'s 2022 study will need to be performed, as well as different SAI experiment designs.

Not all regions have signal-to-noise ratios that are above 1 (Fig S9) or show statistically significant differences between scenarios (Fig 5, S10), which is a common occurrence for sensitive variables such as wind. Despite the ongoing debate surrounding the consistency of Global Circulation Models with observations and their ability to simulate long-term trends (Pryor & Barthelmie, 2010; Pryor et al., 2020; Tian et al., 2019; Sheperd, 2014), particularly in coastal areas (Soares et al., 2017; Solaun & Cerdá, 2019), they are presently the most reliable source for global wind projections with SAI.

Our offshore energy assessment may further incur inaccuracies as a result of overestimating suitable areas by ignoring common shipping lanes and their unsuitability for wind farms. It is likely that for energy generation purposes unsuitable areas such as ports and frequently used transportation routes are located in proximity to areas that we consider particularly suitable, that is, areas close to population centers.

This study looks at the large-scale changes in the dynamics of the circulation system. While these have an important influence on local wind conditions, wind speeds in the lower levels of the atmospheric boundary layer, i.e., those accessible to wind turbines, are highly susceptible to turbulence from small-scale features such as buildings, trees and valleys (Veers et al., 2019). These microscale processes are not resolved in our global analysis. An SSP245-world would likely have substantial differences in terms of land cover and population distribution compared to an SSP585- or an SAI-world. As these things are hard to predict and would complicate the comparison between scenarios, we chose equal area weighting for all scenarios.

Future research should not only consider other types of renewable energy sources such as biofuels and hydropower but look at the effects of SAI on renewable energy sources in conjunction. This would allow to identify regions where not just one RE technology, but potentially several, may experience a change in their productivity with SAI. Additionally, it is relevant to consider not only resource changes due to SRM but also demand changes. One could imagine a modified demand for heating and cooling under SRM, for example. Studies looking at other types of SRM, such as Marine Cloud Brightening, would offer a more complete picture on SRM and renewable energy. At the same time, improvements in the representation of SRM and the response of atmospheric circulation to a change in forcing in the Earth System Models would substantially increase accuracy of the results. Since stratospheric heating has been found to play an important role in changing large-scale circulation (Simpson et al., 2019; Charlesworth et al., 2023, Baldwin & Dunkerton, 2001; Graft et al., 1993; Stenchikov et al. 2002; DallaSanta et al., 2019), narrowing down the uncertainty related to the radiative properties of stratospheric aerosols could improve the understanding of the impacts of SAI on wind RE. And lastly, since SAI seems to significantly affect the spatial distribution of wind resources, regional scale analyses are an essential addition in better understanding wind potential under SAI.

5 Conclusion

Wind renewable energy is considered a critical component in the efforts to reduce greenhouse gas emissions and transition to a more sustainable energy system. Studying the interplay between SAI and wind energy is important to understand whether mitigation and SAI could work together to address climate change. Here, we examined the alterations in wind patterns and RE resources under SAI using the CNRM-ESM2-1.

We find that SAI, while counterbalancing the temperature increase of climate change, does not seem to counterbalance the effects of climate change on wind RE. Instead, our model simulations suggest that SAI may create new atmospheric circulation features (Fig 2-4). The overall long-term impact on WRE resources appears to be highly location-specific, with large increases and reductions in potential under SAI compared to SSP245 or SSP585 of 16 % (Fig 5, S10). However, the long-term total global change in potential is negligible. Furthermore, we find that SAI increases the number of weeks of considerably low production per year in most places around the world (Fig 6) compared to the SSP-scenarios and to the present, although to a much lesser degree than for solar RE (Baur et al., 2023). We note that the reduction in long-term potential and the increase in low energy weeks is not due to an increase of wind speed under SAI (Fig 7).

This paper contributes to the ongoing discourse on climate intervention strategies and their implications for mitigation. While this study entails a high temporal resolution and a fairly high number of ensemble members, future studies could rely on higher spatial resolution models and a larger range of emission scenarios with SAI to test and improve accuracy of the current assumptions. Climate projections are still faced with the challenge of understanding the effect of global warming on atmospheric circulation change and pattern formation (Shepherd, 2014). Improvements in these fundamental understandings might help in attributing the changes from the combined effects of global warming and SAI on wind allowing for a better investigation of the impacts of SAI on WRE potential. We suggest that further research is necessary to assess the wider impacts of SAI on renewable energies to enable more responsible and informed decision-making on climate intervention.

Acknowledgments

Susanne Baur is supported by CERFACS through the project MIRAGE. BS and RS acknowledges funding by the European Union's Horizon 2020 (H2020) research and innovation

program under Grant Agreement No. 101003536 (ESM2025 – Earth System Models for the Future), 821003 (4C, Climate-Carbon Interactions in the Coming Century) and 101003687 (PROVIDE).

Conflict of Interest

The authors declare no conflict of interest.

Open Research

Availability Statement

The code is available at https://github.com/susannebaur/SRM_wind_RE.git. Upon final publication the code will be made publicly available with a DOI under zenodo.

Underlying data is output from the CNRM-ESM2-1 Earth System Model. Due to the large size of the raw data (>1.5TB) it is available upon request from the authors until a sufficiently large storage repository has been found. The post-processed model output will be made available upon final publication with a DOI on zenodo. Land use and land cover as well as population density projections are from the IMAGE3.0-LPJ model (Doelman et al., 2018; Stehfest et al., 2014). Land and ocean protected areas are from the International Union for Conservation of Nature (IUCN, 2023). The Exclusive Economic Zone (EEZ) is from the Flanders Marine Institute (2019), bathymetry and sea-ice information is output from the CNRM-ESM2-1 simulations. Figures were created using the matplotlib library and the matplotlib wrapper proplot.

References

Alizadeh, M. J., Kavianpour, M. R., Kamranzad, B., & Etemad-Shahidi, A. (2020). A distributed wind downscaling technique for wave climate modeling under future scenarios. *Ocean Modelling*, *145*, 101513. https://doi.org/10.1016/j.ocemod.2019.101513

644 Archer, C. L., & Jacobson, M. Z. (2005). Evaluation of global wind power. *Journal of*
645 *Geophysical Research: Atmospheres*, *110*(D12), 2004JD005462.
646 https://doi.org/10.1029/2004JD005462
647 Arent, D., Sullivan, P., Heimiller, D., Lopez, A., Eurek, K., Badger, J., Jorgensen, H.E., Kelly,
648 M., Clarke, L., Luckow, P. (2012). Improved offshore wind resource assessment in global
649 climate stabilization scenarios. NREL/TP-6A20–55049. National Renewable Energy
650 Laboratory, Golden, CO.
651 Aukitino, T., Khan, M. G. M., & Ahmed, M. R. (2017). Wind energy resource assessment for
652 Kiribati with a comparison of different methods of determining Weibull parameters.
653 *Energy Conversion and Management*, *151*, 641–660.
654 https://doi.org/10.1016/j.enconman.2017.09.027
655 Baldwin, M. P., & Dunkerton, T. J. (2001). Stratospheric Harbingers of Anomalous Weather
656 Regimes, *294*.
657 Barnes, E. A., Solomon, S., & Polvani, L. M. (2016). Robust Wind and Precipitation Responses
658 to the Mount Pinatubo Eruption, as Simulated in the CMIP5 Models. *Journal of Climate*,
659 *29*(13), 4763–4778. https://doi.org/10.1175/JCLI-D-15-0658.1
660 Baur, S., Sanderson, B. M., Séférian, R., & Terray, L. (2023). Solar Radiation Modification
661 challenges decarbonization with renewable solar energy (preprint). *Earth System*
662 *Dynamics*. https://doi.org/10.5194/egusphere-2023-2337.
663 Bosch, J., Staffell, I., & Hawkes, A. D. (2017). Temporally-explicit and spatially-resolved global
664 onshore wind energy potentials. *Energy*, *131*, 207–217.
665 https://doi.org/10.1016/j.energy.2017.05.052
666 Burton, T., Sharpe, D., Jenkins, N., Bossanyi, E. (2001). Wind energy handbook. *John Wiley &*
667 *Sons*. DOI:10.1002/0470846062
668 Carrillo, C., Obando Montaño, A. F., Cidrás, J., & Díaz-Dorado, E. (2013). Review of power
669 curve modelling for wind turbines. *Renewable and Sustainable Energy Reviews*, *21*, 572–
670 581. https://doi.org/10.1016/j.rser.2013.01.012
671 Carvalho, D., Rocha, A., Gómez-Gesteira, M., & Silva Santos, C. (2017). Potential impacts of
672 climate change on European wind energy resource under the CMIP5 future climate
673 projections. *Renewable Energy*, *101*, 29–40. https://doi.org/10.1016/j.renene.2016.08.036
674 Chang, T.-J., Chen, C.-L., Tu, Y.-L., Yeh, H.-T., & Wu, Y.-T. (2015). Evaluation of the climate
675 change impact on wind resources in Taiwan Strait. *Energy Conversion and Management*,
676 *95*, 435–445. https://doi.org/10.1016/j.enconman.2015.02.033
677 Charlesworth, E., Plöger, F., Birner, T., Baikhadzhaev, R., Abalos, M., Abraham, N. L., et al.
678 (2023). Stratospheric water vapor affecting atmospheric circulation. *Nature*
679 *Communications*, *14*(1), 3925. https://doi.org/10.1038/s41467-023-39559-2
680 Cheng, W., MacMartin, D. G., Dagon, K., Kravitz, B., Tilmes, S., Richter, J. H., et al. (2019).
681 Soil Moisture and Other Hydrological Changes in a Stratospheric Aerosol
682 Geoengineering Large Ensemble. *Journal of Geophysical Research: Atmospheres*,
683 *124*(23), 12773–12793. https://doi.org/10.1029/2018JD030237
684 Chu, C.-T., & Hawkes, A. D. (2020). A geographic information system-based global variable
685 renewable potential assessment using spatially resolved simulation. *Energy*, *193*, 116630.
686 https://doi.org/10.1016/j.energy.2019.116630
687 Clarke, L., Wei, Y.-M., De La Vega Navarro, A., Garg, A., Hahmann, A.N., Khennas, S.,
688 Azevedo, I.M.L., Löschel, A., Singh, A.K., Steg, L., Strbac, G., Wada, K. (2022). Energy
689 Systems. In IPCC, 2022: Climate Change 2022: Mitigation of Climate Change.

690 Contribution of Working Group III to the Sixth Assessment Report of the
691 Intergovernmental Panel on Climate Change [P.R. Shukla, J. Skea, R. Slade, A. Al
692 Khourdajie, R. van Diemen, D. McCollum, M. Pathak, S. Some, P. Vyas, R. Fradera, M.
693 Belkacemi, A. Hasija, G. Lisboa, S. Luz, J. Malley, (eds.)]. *Cambridge University Press,*
694 *Cambridge, UK and New York, NY, USA*. doi: 10.1017/9781009157926.008
695 Cradden, L., Restuccia, F., Hawkins, S., & Harrison, G. (2014). Consideration of Wind Speed
696 Variability in Creating a Regional Aggregate Wind Power Time Series. *Resources*, *3*(1),
697 215–234. https://doi.org/10.3390/resources3010215
698 Da-Allada, C. Y., Baloïtcha, E., Alamou, E. A., Awo, F. M., Bonou, F., Pomalegni, Y., et al.
699 (2020). Changes in West African Summer Monsoon Precipitation Under Stratospheric
700 Aerosol Geoengineering. *Earth's Future*, *8*(7), e2020EF001595.
701 https://doi.org/10.1029/2020EF001595
702 Dai, Z., Weisenstein, D. K., & Keith, D. W. (2018). Tailoring Meridional and Seasonal Radiative
703 Forcing by Sulfate Aerosol Solar Geoengineering. *Geophysical Research Letters*, *45*(2),
704 1030–1039. https://doi.org/10.1002/2017GL076472
705 DallaSanta, K., Gerber, E. P., & Toohey, M. (2019). The Circulation Response to Volcanic
706 Eruptions: The Key Roles of Stratospheric Warming and Eddy Interactions. *Journal of*
707 *Climate*, *32*(4), 1101–1120. https://doi.org/10.1175/JCLI-D-18-0099.1
708 Davy, R., Gnatiuk, N., Pettersson, L., & Bobylev, L. (2018). Climate change impacts on wind
709 energy potential in the European domain with a focus on the Black Sea. *Renewable and*
710 *Sustainable Energy Reviews*, *81*, 1652–1659. https://doi.org/10.1016/j.rser.2017.05.253
711 De Jong, P., Barreto, T. B., Tanajura, C. A. S., Kouloukoui, D., Oliveira-Esquerre, K. P.,
712 Kiperstok, A., & Torres, E. A. (2019). Estimating the impact of climate change on wind
713 and solar energy in Brazil using a South American regional climate model. *Renewable*
714 *Energy*, *141*, 390–401. https://doi.org/10.1016/j.renene.2019.03.086
715 Doelman, J. C., Stehfest, E., Tabeau, A., Van Meijl, H., Lassaletta, L., Gernaat, D. E. H. J., et al.
716 (2018). Exploring SSP land-use dynamics using the IMAGE model: Regional and
717 gridded scenarios of land-use change and land-based climate change mitigation. *Global*
718 *Environmental Change*, *48*, 119–135. https://doi.org/10.1016/j.gloenvcha.2017.11.014
719 Dvorak, M. J., Archer, C. L., & Jacobson, M. Z. (2010). California offshore wind energy
720 potential. *Renewable Energy*, *35*(6), 1244–1254.
721 https://doi.org/10.1016/j.renene.2009.11.022
722 Elliot, D., Schwartz, M. (1993). Wind energy potential in the United States. *Pacific Northwest*
723 *Laboratory*.
724 Elsner, P. (2019). Continental-scale assessment of the African offshore wind energy potential:
725 Spatial analysis of an under-appreciated renewable energy resource. *Renewable and*
726 *Sustainable Energy Reviews*, *104*, 394–407. https://doi.org/10.1016/j.rser.2019.01.034
727 Eskin, N., Artar, H., & Tolun, S. (2008). Wind energy potential of Gökçeada Island in Turkey.
728 *Renewable and Sustainable Energy Reviews*, *12*(3), 839–851.
729 https://doi.org/10.1016/j.rser.2006.05.016
730 Eurek, K., Sullivan, P., Gleason, M., Hettinger, D., Heimiller, D., & Lopez, A. (2017). An
731 improved global wind resource estimate for integrated assessment models. *Energy*
732 *Economics*, *64*, 552–567. https://doi.org/10.1016/j.eneco.2016.11.015
733 Flanders Marine Institute (2019). Maritime Boundaries Geodatabase: Maritime Boundaries and
734 Exclusive Economic Zones (200NM), version 11. Available online at
735 https://www.marineregions.org/. Last accessed: 05. April 2023.

Gernaat, D. E. H. J., de Boer, H. S., Daioglou, V., Yalew, S. G., Müller, C., & van Vuuren, D. P. (2021). Climate change impacts on renewable energy supply. *Nature Climate Change*, *11*(2), 119–125. https://doi.org/10.1038/s41558-020-00949-9

Graf, H.-F. (1992). Arctic radiation deficit and climate variability. *Climate Dynamics*, 7, 19–28, https://doi.org/10.1007/BF00204818.

Graft, H.-F., Kirchner, I., Robock, A. (1993). Pinatubo eruption winter climate effects: model versus observations. *Climate Dynamics,* 9, 81–93. https://doi.org/10.1007/BF00210011

Hoogwijk, M. M. (2004). *On the global and regional potential of renewable energy sources = Over het mondiale en regionale potentieel van hernieuwbare energiebronnen*. Universiteit Utrecht, Faculteit Scheikunde, Utrecht.

Horton, J. B. (2015). The emergency framing of solar geoengineering: Time for a different approach. *The Anthropocene Review*, *2*(2), 147–151. https://doi.org/10.1177/2053019615579922

IPCC (2018). Summary for Policymakers. In: Global Warming of 1.5°C. An IPCC Special Report on the impacts of global warming of 1.5°C above pre-industrial levels and related global greenhouse gas emission pathways, in the context of strengthening the global response to the threat of climate change, sustainable development, and efforts to eradicate poverty [Masson-Delmotte, V., P. Zhai, H.-O. Pörtner, D. Roberts, J. Skea, P.R. Shukla, A. Pirani, W. Moufouma-Okia, C. Péan, R. Pidcock, S. Connors, J.B.R. Matthews, Y. Chen, X. Zhou, M.I. Gomis, E. Lonnoy, T. Maycock, M. Tignor, and T. Waterfield (eds.)]. *Cambridge University Press, Cambridge, UK and New York, NY, USA*, 3-24. https://doi.org/10.1017/9781009157940.001

IUCN (International Union for Conservation of Nature) (2023). The World Database on Protected Areas (WDPA).

Jung, C., & Schindler, D. (2022). A review of recent studies on wind resource projections under climate change. *Renewable and Sustainable Energy Reviews*, *165*, 112596. https://doi.org/10.1016/j.rser.2022.112596

Jung, C., Schindler, D., & Laible, J. (2018). National and global wind resource assessment under six wind turbine installation scenarios. *Energy Conversion and Management*, *156*, 403–415. https://doi.org/10.1016/j.enconman.2017.11.059

Justus, C.G., Hargraves, W.R., Mikhail, A. & Graber, D. (1978). Methods for estimating wind speed frequency distributions. *J. Appl. Meteorol.*, 17, 350–353.

Karpechko, A. Yu., Gillett, N. P., Dall'Amico, M., & Gray, L. J. (2010). Southern Hemisphere atmospheric circulation response to the El Chichón and Pinatubo eruptions in coupled climate models: Southern Hemisphere Response to El Chichón and Pinatubo. *Quarterly Journal of the Royal Meteorological Society*, *136*(652), 1813–1822. https://doi.org/10.1002/qj.683

Kirchner, I., Stenchikov, G. L., Graf, H.-F., Robock, A. & Antufia, J. C. (1999). Climate model simulation of winter warming and summer cooling following the 1991 Mount Pinatubo volcanic eruption. *J. Geophys. Res.*, 104, 19 039–19 055, https://doi.org/10.1029/1999JD900213.

Kravitz, B., Robock, A., Tilmes, S., Boucher, O., English, J. M., Irvine, P. J., et al. (2015). The Geoengineering Model Intercomparison Project Phase 6 (GeoMIP6): Simulation design and preliminary results. *Geoscientific Model Development*, *8*(10), 3379–3392. https://doi.org/10.5194/gmd-8-3379-2015

781 Kravitz, Ben, MacMartin, D. G., Wang, H., & Rasch, P. J. (2016). Geoengineering as a design
782 problem. *Earth System Dynamics*, *7*(2), 469–497. https://doi.org/10.5194/esd-7-469-2016
783 Kravitz, Ben, MacMartin, D. G., Tilmes, S., Richter, J. H., Mills, M. J., Cheng, W., et al.
784 (2019a). Comparing Surface and Stratospheric Impacts of Geoengineering With Different
785 SO $_2$ Injection Strategies. *Journal of Geophysical Research: Atmospheres*, *124*(14),
786 7900–7918. https://doi.org/10.1029/2019JD030329
787 Kravitz, Ben, MacMartin, D. G., Tilmes, S., Richter, J. H., Mills, M. J., Cheng, W., et al.
788 (2019b). Comparing Surface and Stratospheric Impacts of Geoengineering With Different
789 SO $_2$ Injection Strategies. *Journal of Geophysical Research: Atmospheres*, *124*(14),
790 7900–7918. https://doi.org/10.1029/2019JD030329
791 Krewitt, W., K. Nienhaus, C. Kleßmann, C. Capone, E. Stricker, W. Graus, M. Hoogwijk, N.
792 Supersberger, U. von Winterfeld & Samadi, S. (2009). Role and Potential of Renewable
793 Energy and Energy Efficiency for Global Energy Supply. *Climate Change*, 18, 336, ISSN
794 1862-4359, Federal Environment Agency, Dessau-Roßlau, Germany.
795 Lee, H., Muri, H., Ekici, A., Tjiputra, J., & Schwinger, J. (2020). The response of terrestrial
796 ecosystem carbon cycling under different aerosol-based radiation management
797 geoengineering. *Earth System Dynamics*, (July). https://doi.org/10.5194/esd-2020-57
798 Lee, J. C. Y., Fields, M. J., & Lundquist, J. K. (2018). Assessing variability of wind speed:
799 comparison and validation of 27 methodologies. *Wind Energy Science*, *3*(2), 845–868.
800 https://doi.org/10.5194/wes-3-845-2018
801 Li, Y., Huang, X., Tee, K. F., Li, Q., & Wu, X.-P. (2020). Comparative study of onshore and
802 offshore wind characteristics and wind energy potentials: A case study for southeast
803 coastal region of China. *Sustainable Energy Technologies and Assessments*, *39*, 100711.
804 https://doi.org/10.1016/j.seta.2020.100711
805 Liu, Z., Lang, X., Miao, J., & Jiang, D. (2023). Impact of Stratospheric Aerosol Injection on the
806 East Asian Winter Monsoon. *Geophysical Research Letters*, *50*(3), e2022GL102109.
807 https://doi.org/10.1029/2022GL102109
808 Lu, X., M.B. McElroy & Kiviluoma, J. (2009). Global potential for wind-generated electricity.
809 *Proceedings of the National Academy of Sciences,* 106, 10933- 10939.
810 Lysen, E. H. (1983). Introduction to Wind Energy. *CWD Publication, The Netherlands*, No.
811 CWD 82–1.
812 Ma, J., Xie, S.-P., & Kosaka, Y. (2012). Mechanisms for Tropical Tropospheric Circulation
813 Change in Response to Global Warming*. *Journal of Climate*, *25*(8), 2979–2994.
814 https://doi.org/10.1175/JCLI-D-11-00048.1
815 MacCracken, M. C. (2009). On the possible use of geoengineering to moderate specific climate
816 change impacts. *Environmental Research Letters*, *4*(4), 045107.
817 https://doi.org/10.1088/1748-9326/4/4/045107
818 MacMartin, D. G., & Kravitz, B. (2019). The Engineering of Climate Engineering. *Annual*
819 *Review of Control, Robotics, and Autonomous Systems*, *2*(1), 445–467.
820 https://doi.org/10.1146/annurev-control-053018-023725
821 Marshall, A. G., Scaife, A. A., & Ineson, S. (2009). Enhanced Seasonal Prediction of European
822 Winter Warming following Volcanic Eruptions. *Journal of Climate*, *22*(23), 6168–6180.
823 https://doi.org/10.1175/2009JCLI3145.1
824 Martinez, A., & Iglesias, G. (2024). Global wind energy resources decline under climate change.
825 *Energy*, *288*, 129765. https://doi.org/10.1016/j.energy.2023.129765

McCusker, K. E., Battisti, D. S., & Bitz, C. M. (2015). Inability of stratospheric sulfate aerosol injections to preserve the West Antarctic Ice Sheet. *Geophysical Research Letters*, *42*(12), 4989–4997. https://doi.org/10.1002/2015GL064314

McCusker, Kelly E., Armour, K. C., Bitz, C. M., & Battisti, D. S. (2014). Rapid and extensive warming following cessation of solar radiation management. *Environmental Research Letters*, *9*(2). https://doi.org/10.1088/1748-9326/9/2/024005

McGraw, M. C., Barnes, E. A., & Deser, C. (2016). Reconciling the observed and modeled Southern Hemisphere circulation response to volcanic eruptions. *Geophysical Research Letters*, *43*(13), 7259–7266. https://doi.org/10.1002/2016GL069835

Mohammadi, K., Alavi, O., Mostafaeipour, A., Goudarzi, N., & Jalilvand, M. (2016). Assessing different parameters estimation methods of Weibull distribution to compute wind power density. *Energy Conversion and Management*, *108*, 322–335. https://doi.org/10.1016/j.enconman.2015.11.015

Mousavi, S. V., Karami, K., Tilmes, S., Muri, H., Xia, L., & Rezaei, A. (2023). Future dust concentration over the Middle East and North Africa region under global warming and stratospheric aerosol intervention scenarios. *Atmospheric Chemistry and Physics*, *23*(18), 10677–10695. https://doi.org/10.5194/acp-23-10677-2023

Müller-Hansen, F., Repke, T., Baum, C. M., Brutschin, E., Callaghan, M. W., Debnath, R., et al. (2023). Attention, sentiments and emotions towards emerging climate technologies on Twitter. *Global Environmental Change*, *83*, 102765. https://doi.org/10.1016/j.gloenvcha.2023.102765

O'Neill, B. C., Tebaldi, C., Van Vuuren, D. P., Eyring, V., Friedlingstein, P., Hurtt, G., et al. (2016). The Scenario Model Intercomparison Project (ScenarioMIP) for CMIP6. *Geoscientific Model Development*, *9*(9), 3461–3482. https://doi.org/10.5194/gmd-9-3461-2016

Pereira De Lucena, A. F., Szklo, A. S., Schaeffer, R., & Dutra, R. M. (2010). The vulnerability of wind power to climate change in Brazil. *Renewable Energy*, *35*(5), 904–912. https://doi.org/10.1016/j.renene.2009.10.022

Pereira, E. B., Martins, F. R., Pes, M. P., Da Cruz Segundo, E. I., & Lyra, A. D. A. (2013). The impacts of global climate changes on the wind power density in Brazil. *Renewable Energy*, *49*, 107–110. https://doi.org/10.1016/j.renene.2012.01.053

Perrin, O., Rootzén, H., & Taesler, R. (2006). A Discussion of Statistical Methods Used to Estimate Extreme Wind Speeds. *Theor. Appl. Climatol,* 85(3-4), 203–215. doi:10.1007/s00704-005-0187-3

Polvani, L. M., & Kushner, P. J. (2002). Tropospheric response to stratospheric perturbations in a relatively simple general circulation model. *Geophysical Research Letters*, *29*(7). https://doi.org/10.1029/2001GL014284

Pryor, S. C., Nielsen, M., Barthelmie, R. J. & Mann, J. (2004). Can satellite sampling of offshore wind speeds realistically represent wind speed distributions? Part II: Quantifying uncertainties associated with sampling strategy and distribution fitting methods. *J. Appl. Meteorol.*, 43, 739–750.

Pryor, S.C., R.J. Barthelmie, D.T. Young, E.S. Takle, R.W. Arritt, D. Flory, W. Gutowski Jr., A. Nunes & Roads, J. (2009). Wind speed trends over the contiguous United States. *Journal of Geophysical Research – Atmospheres*, 114, D14105.

Pryor, S. C., & Barthelmie, R. J. (2010). Climate change impacts on wind energy: A review. *Renewable and Sustainable Energy Reviews*, *14*(1), 430–437. https://doi.org/10.1016/j.rser.2009.07.028

Pryor, S. C., Barthelmie, R. J., Bukovsky, M. S., Leung, L. R., & Sakaguchi, K. (2020). Climate change impacts on wind power generation. *Nature Reviews Earth & Environment*, *1*(12), 627–643. https://doi.org/10.1038/s43017-020-0101-7

Ramachandran, S., Ramaswamy, V., Stenchikov, G. L., & Robock, A. (2000). Radiative impact of the Mount Pinatubo volcanic eruption: Lower stratospheric response. *Journal of Geophysical Research: Atmospheres*, *105*(D19), 24409–24429. https://doi.org/10.1029/2000JD900355

Riahi, K., Schaeffer, R., Arango, J., Calvin, K., Guivarch, C., Hasegawa, T., Jiang, K., Kriegler, E., Matthews, R., Peters, G.P., Rao, A., Robertson, S., Sebbit, A.M., Steinberger, J., Tavoni, M., van Vuuren, D.P. (2022). Mitigation pathways compatible with long-term goals. In IPCC, 2022: Climate Change 2022: Mitigation of Climate Change. Contribution of Working Group III to the Sixth Assessment Report of the Intergovernmental Panel on Climate Change [P.R. Shukla, J. Skea, R. Slade, A. Al Khourdajie, R. van Diemen, D. McCollum, M. Pathak, S. Some, P. Vyas, R. Fradera, M. Belkacemi, A. Hasija, G. Lisboa, S. Luz, J. Malley, (eds.)]. *Cambridge University Press, Cambridge, UK and New York, NY, USA*. doi: 10.1017/9781009157926.005

Ripple, W. J., Wolf, C., Gregg, J. W., Rockström, J., Newsome, T. M., Law, B. E., et al. (2023). The 2023 state of the climate report: Entering uncharted territory. *BioScience*, *73*(12), 841–850. https://doi.org/10.1093/biosci/biad080

Robock, A., Adams, T., Moore, M., Oman, L., & Stenchikov, G. (2007). Southern Hemisphere atmospheric circulation effects of the 1991 Mount Pinatubo eruption. *Geophysical Research Letters*, *34*(23), 2007GL031403. https://doi.org/10.1029/2007GL031403

Robock, A., Oman, L., & Stenchikov, G. L. (2008). Regional climate responses to geoengineering with tropical and Arctic SO2 injections. *Journal of Geophysical Research Atmospheres*, *113*(16), 1–15. https://doi.org/10.1029/2008JD010050

Roscoe, H. K., & Haigh, J. D. (2007). Influences of ozone depletion, the solar cycle and the QBO on the Southern Annular Mode: INFLUENCES ON THE SOUTHERN ANNULAR MODE. *Quarterly Journal of the Royal Meteorological Society*, *133*(628), 1855–1864. https://doi.org/10.1002/qj.153

Royal Society. (2011). *Solar Radiation Management: The Governance of Research* (p. 70). London, UK: The Royal Society of London. Retrieved from https://royalsociety.org/-/media/Royal_Society_Content/policy/projects/solar-radiation-governance/DES2391_SRMGI-report_web.pdf

Saint-Drenan, Y.-M., Besseau, R., Jansen, M., Staffell, I., Troccoli, A., Dubus, L., et al. (2020). A parametric model for wind turbine power curves incorporating environmental conditions. *Renewable Energy*, *157*, 754–768. https://doi.org/10.1016/j.renene.2020.04.123

Sawadogo, W., Reboita, M. S., Faye, A., da Rocha, R. P., Odoulami, R. C., Olusegun, C. F., et al. (2021). Current and future potential of solar and wind energy over Africa using the RegCM4 CORDEX-CORE ensemble. *Climate Dynamics*, *57*(5), 1647–1672. https://doi.org/10.1007/s00382-020-05377-1

Schäfer, S., Stelzer, H., Maas, A., & Lawrence, M. G. (2014). Earth's future in the Anthropocene: Technological interventions between piecemeal and utopian social engineering. *Earth's Future*, *2*(4), 239–243. https://doi.org/10.1002/2013EF000190

Séférian, R., Nabat, P., Michou, M., Saint-Martin, D., Voldoire, A., Colin, J., et al. (2019). Evaluation of CNRM Earth System Model, CNRM-ESM2-1: Role of Earth System Processes in Present-Day and Future Climate. *Journal of Advances in Modeling Earth Systems*, *11*(12), 4182–4227. https://doi.org/10.1029/2019MS001791

Shaw, T. A., Baldwin, M., Barnes, E. A., Caballero, R., Garfinkel, C. I., Hwang, Y.-T., et al. (2016). Storm track processes and the opposing influences of climate change. *Nature Geoscience*, *9*(9), 656–664. https://doi.org/10.1038/ngeo2783

Shepherd, T. (2014). Atmospheric circulation as a source of uncertainty in climate change projections. *Nature Geosci*., 7, 703–708. https://doi-org.insu.bib.cnrs.fr/10.1038/ngeo2253

Shi, H., Dong, Z., Xiao, N., & Huang, Q. (2021). Wind Speed Distributions Used in Wind Energy Assessment: A Review. *Frontiers in Energy Research*, *9*. Retrieved from https://www.frontiersin.org/articles/10.3389/fenrg.2021.769920

Shin, J.-Y., Jeong, C., & Heo, J.-H. (2018). A Novel Statistical Method to Temporally Downscale Wind Speed Weibull Distribution Using Scaling Property. *Energies*, *11*(3), 633. https://doi.org/10.3390/en11030633

Shu, Z. R., & Jesson, M. (2021). Estimation of Weibull parameters for wind energy analysis across the UK. *Journal of Renewable and Sustainable Energy*, *13*(2), 023303. https://doi.org/10.1063/5.0038001

Shu, Z. R., Li, Q. S., & Chan, P. W. (2015). Investigation of offshore wind energy potential in Hong Kong based on Weibull distribution function. *Applied Energy*, *156*, 362–373. https://doi.org/10.1016/j.apenergy.2015.07.027

Simpson, I. R., Tilmes, S., Richter, J. H., Kravitz, B., MacMartin, D. G., Mills, M. J., et al. (2019). The Regional Hydroclimate Response to Stratospheric Sulfate Geoengineering and the Role of Stratospheric Heating. *Journal of Geophysical Research: Atmospheres*, *124*(23), 12587–12616. https://doi.org/10.1029/2019JD031093

Simpson, Isla R., Blackburn, M., & Haigh, J. D. (2009). The Role of Eddies in Driving the Tropospheric Response to Stratospheric Heating Perturbations. *Journal of the Atmospheric Sciences*, *66*(5), 1347–1365. https://doi.org/10.1175/2008JAS2758.1

Soares, P. M. M., Lima, D. C. A., Cardoso, R. M., Nascimento, M. L., & Semedo, A. (2017). Western Iberian offshore wind resources: More or less in a global warming climate? *Applied Energy*, *203*, 72–90. https://doi.org/10.1016/j.apenergy.2017.06.004

Sohoni, V., Gupta, S. C., & Nema, R. K. (2016). A Critical Review on Wind Turbine Power Curve Modelling Techniques and Their Applications in Wind Based Energy Systems. *Journal of Energy*, *2016*, 1–18. https://doi.org/10.1155/2016/8519785

Solaun, K., & Cerdá, E. (2019). Climate change impacts on renewable energy generation. A review of quantitative projections. *Renewable and Sustainable Energy Reviews*, *116*. https://doi.org/10.1016/j.rser.2019.109415

Stehfest, E., Van Vuuren, D., Kram, T., Bouwman, L., Alkemade, R., Bakkenes, M., Biemans, H., Bouwman, A., Den Elzen, M., Janse, J., Lucas, P., Van Minnen, J., Müller, C. & Prins, A. (2014). Integrated Assessment of Global Environmental Change with IMAGE 3.0. Model Description and Policy Applications, *Netherlands Environmental Assessment Agency (The Hague)*, ISBN: 978-94-91506-71-0

960 Stenchikov, G., Robock, A., Ramaswamy, V., Schwarzkopf, M. D., Hamilton, K., &
961 Ramachandran, S. (2002). Arctic Oscillation response to the 1991 Mount Pinatubo
962 eruption: Effects of volcanic aerosols and ozone depletion. *Journal of Geophysical*
963 *Research: Atmospheres*, *107*(D24). https://doi.org/10.1029/2002JD002090
964 Tang, W., Tilmes, S., Lawrence, D. M., Li, F., He, C., Emmons, L. K., et al. (2023). Impact of
965 solar geoengineering on wildfires in the 21st century in CESM2/WACCM6. *Atmospheric*
966 *Chemistry and Physics*, *23*(9), 5467–5486. https://doi.org/10.5194/acp-23-5467-2023
967 Tian, Q., Huang, G., Hu, K., & Niyogi, D. (2019). Observed and global climate model based
968 changes in wind power potential over the Northern Hemisphere during 1979–2016.
969 *Energy*, *167*, 1224–1235. https://doi.org/10.1016/j.energy.2018.11.027
970 Tilmes, S., Mills, M. J., Niemeier, U., Schmidt, H., Robock, A., Kravitz, B., et al. (2015). A new
971 Geoengineering Model Intercomparison Project (GeoMIP) experiment designed for
972 climate and chemistry models. *Geoscientific Model Development*, *8*(1), 43–49.
973 https://doi.org/10.5194/gmd-8-43-2015
974 Tilmes, Simone, Richter, J. H., Mills, M. J., Kravitz, B., Macmartin, D. G., Vitt, F., et al. (2017).
975 Sensitivity of aerosol distribution and climate response to stratospheric SO2 injection
976 locations. *Journal of Geophysical Research: Atmospheres*, *122*(23), 12,591-12,615.
977 https://doi.org/10.1002/2017JD026888
978 Tilmes, Simone, Richter, J. H., Kravitz, B., Macmartin, D. G., Mills, M. J., Simpson, I. R., et al.
979 (2018a). CESM1(WACCM) stratospheric aerosol geoengineering large ensemble project.
980 *Bulletin of the American Meteorological Society*, *99*(11), 2361–2371.
981 https://doi.org/10.1175/BAMS-D-17-0267.1
982 Tilmes, Simone, Richter, J. H., Mills, M. J., Kravitz, B., MacMartin, D. G., Garcia, R. R., et al.
983 (2018b). Effects of Different Stratospheric SO_2 Injection Altitudes on Stratospheric
984 Chemistry and Dynamics. *Journal of Geophysical Research: Atmospheres*, *123*(9), 4654–
985 4673. https://doi.org/10.1002/2017JD028146
986 Tobin, I., Greuell, W., Jerez, S., Ludwig, F., Vautard, R., Van Vliet, M. T. H., & Breón, F. M.
987 (2018). Vulnerabilities and resilience of European power generation to 1.5 °c, 2 °c and 3
988 °c warming. *Environmental Research Letters*, *13*(4). https://doi.org/10.1088/1748-
989 9326/aab211
990 Tobin, Isabelle, Vautard, R., Balog, I., Bréon, F. M., Jerez, S., Ruti, P. M., et al. (2015).
991 Assessing climate change impacts on European wind energy from ENSEMBLES high-
992 resolution climate projections. *Climatic Change*, *128*(1–2), 99–112.
993 https://doi.org/10.1007/s10584-014-1291-0
994 Tye, M. R., Stephenson, D. B., Holland, G. J., & Katz, R. W. (2014). A Weibull Approach for
995 Improving Climate Model Projections of Tropical Cyclone Wind-Speed Distributions.
996 *Journal of Climate*, *27*(16), 6119–6133. https://doi.org/10.1175/JCLI-D-14-00121.1
997 Valencia Ochoa, G., Núñez Alvarez, J., & Vanegas Chamorro, M. (2019). Data set on wind
998 speed, wind direction and wind probability distributions in Puerto Bolivar - Colombia.
999 *Data in Brief*, *27*, 104753. https://doi.org/10.1016/j.dib.2019.104753
1000 Vautard, R., Cattiaux, J., Yiou, P., Thépaut, J.-N., & Ciais, P. (2010). Northern Hemisphere
1001 atmospheric stilling partly attributed to an increase in surface roughness. *Nature*
1002 *Geoscience*, *3*(11), 756–761. https://doi.org/10.1038/ngeo979
1003 Veers, P., Dykes, K., Lantz, E., Barth, S., Bottasso, C. L., Carlson, O., et al. (2019). Grand
1004 challenges in the science of wind energy. *Science*, *366*(6464), eaau2027.
1005 https://doi.org/10.1126/science.aau2027

Veronesi, F., & Grassi, S. (2015). Comparison of hourly and daily wind speed observations for the computation of Weibull parameters and power output. In *2015 3rd International Renewable and Sustainable Energy Conference (IRSEC)* (pp. 1–6). Marrakech, Morocco: IEEE. https://doi.org/10.1109/IRSEC.2015.7455043

Vestas (2023a). V236-15.0 MW™. https://www.vestas.com/en/products/offshore/V236-15MW. Last accessed: 24. January 2024.

Vestas (2023b). V162-6.2 MW™. https://www.vestas.com/en/products/enventus-platform/v162-6-2-mw. Last accessed: 24. January 2024.

de Vries, B. J. M., van Vuuren, D. P., & Hoogwijk, M. M. (2007). Renewable energy sources: Their global potential for the first-half of the 21st century at a global level: An integrated approach. *Energy Policy*, *35*(4), 2590–2610. https://doi.org/10.1016/j.enpol.2006.09.002

Wood, A.J. and Wollenberg, B. (1996) Power Generation Operation and Control. 2nd Edition. *Fuel and Energy Abstracts*, *Elsevier*, 37(3), 195.

Xie, M., Moore, J. C., Zhao, L., Wolovick, M., & Muri, H. (2022). Impacts of three types of solar geoengineering on the Atlantic Meridional Overturning Circulation. *Atmospheric Chemistry and Physics*, *22*(7), 4581–4597. https://doi.org/10.5194/acp-22-4581-2022

Yan, B., Chan, P. W., Li, Q. S., He, Y. C., & Shu, Z. R. (2020). Characterising the fractal dimension of wind speed time series under different terrain conditions. *Journal of Wind Engineering and Industrial Aerodynamics*, *201*, 104165. https://doi.org/10.1016/j.jweia.2020.104165

Zeng, Z., Ziegler, A.D., Searchinger, T., Yang, L., Chen, A., Ju, K. et al. (2019). A reversal in global terrestrial stilling and its implications for wind energy production. *Nat Clim Change*, 9, 979–85. https://doi.org/10.1038/s41558-019-0622-6

Zhou, Y., & Smith, S. J. (2013). Spatial and temporal patterns of global onshore wind speed distribution. *Environmental Research Letters*, *8*(3), 034029. https://doi.org/10.1088/1748-9326/8/3/034029

Zhou, Y., Luckow, P., Smith, S. J., & Clarke, L. (2012). Evaluation of Global Onshore Wind Energy Potential and Generation Costs. *Environmental Science & Technology*, *46*(14), 7857–7864. https://doi.org/10.1021/es204706m